The Astrophysical Journal, 616:1078–1085, 2004 December 1

THE PROMPT X-RAY EMISSION OF GRB 011211: POSSIBLE EVIDENCE OF A TRANSIENT ABSORPTION FEATURE

F. Frontera,[1,2] L. Amati,[2] J. J. M. in 't Zand,[3] D. Lazzati,[4] A. Königl,[5] M. Vietri,[6] E. Costa,[7] M. Feroci,[7] C. Guidorzi,[1] E. Montanari,[1] M. Orlandini,[2] E. Pian,[8] and L. Piro[7]

Received 2003 October 21; accepted 2004 August 11

ABSTRACT

We report observation results of the prompt X- and gamma-ray emission from GRB 011211. This event was detected with the Gamma-Ray Burst Monitor and one of the wide-field cameras aboard the *BeppoSAX* satellite. The optical counterpart of the gamma-ray burst was soon identified and its redshift determined ($z = 2.140$), while the X-ray afterglow emission was detected with the *XMM-Newton* satellite. Evidence of soft X-ray emission lines was reported by Reeves and colleagues but not confirmed by other authors. In investigating the spectral evolution of the prompt emission, we find the possible evidence of a transient absorption feature at $6.9^{+0.6}_{-0.5}$ keV during the rise of the primary event. The significance of the feature is derived with nonparametric tests and numerical simulations, finding a chance probability that ranges from 3×10^{-3} down to 4×10^{-4}. The feature shows a Gaussian profile and an equivalent width of $1.2^{+0.5}_{-0.6}$ keV. We discuss our results and their possible interpretation.

Subject headings: gamma rays: bursts — gamma rays: observations — X-rays: general

1. INTRODUCTION

The nature of the progenitors of celestial gamma-ray bursts (GRBs) still is an open issue. Collapse of massive, fast-rotating stars (hypernova model; e.g., Paczynski 1998) or delayed collapse of a rotationally stabilized neutron star (supranova model; Vietri & Stella 1998) are among the favored scenarios for the origin of these events. Both models predict that the preburst environment consists of a high-density gas due to strong winds from the massive progenitor in the case of a hypernova or to a substantial enrichment of heavy elements by a previous supernova (SN) explosion in the case of the supranova model (Lazzati et al. 1999; Böttcher 2000; Weth et al. 2000). The recent discovery from the spectral evolution of the optical afterglow emission from GRB 030329 of a direct connection between this burst and the Type Ic energetic supernova (hypernova) SN 2003dh (e.g., Stanek et al. 2003; Hjorth et al. 2003) seems to point toward the hypernova model, even if the strict simultaneity of the two events has not been fully proved. However, it is not yet clear whether all GRBs are connected to energetic SNe, with many cases lacking evidence of SN spectroscopic features and/or a "supernova bump" in the optical emission of GRB afterglows. On the other hand, from the current estimates of the opening angles of GRB jets, the expected GRB rates, when compared with those of Type Ib/c SNe, suggest that <1% of such SNe might be accompanied by a GRB (Frail et al. 2001). The case of SN 2002ap (e.g., Wang et al. 2003) is an outstanding example of a Type Ic hypernova that has no simultaneous detected GRB event associated with it.

The presence of a postsupernova environment can be tested from the study of the burst X-ray spectrum, which should show a low-energy cutoff and/or absorption features due to elements in the circumburst material left by the previous supernova explosion. Either the progressive photoionization of the neutral gas by the GRB photons (e.g., Perna & Loeb 1998; Böttcher et al. 1999; Lazzati & Perna 2002) or the electron density decrease or the electron temperature increase of an already almost photoionized medium (Lazzati et al. 2001) would make the features transient.

In fact, a transient absorption feature at 3.8 ± 0.3 keV has been detected in the prompt emission X-ray spectrum of GRB 990705 (Amati et al. 2000). The feature is present in the first, rising part of the burst profile and disappears thereafter. Interpreted by Amati et al. (2000) as a cosmologically redshifted K edge due to neutral Fe around the GRB location, a GRB redshift of 0.86 ± 0.17 was derived and later confirmed by optical spectroscopy of the associated host galaxy ($z_{\rm opt} = 0.84$; Le Floc'h et al. 2002). With this assumption, the iron relative abundance with respect to the solar one was derived, $\mathrm{Fe/Fe}_{\odot} = 75 \pm 19$, which is typical of a supernova explosion environment. An alternative explanation was given by Lazzati et al. (2001), who assumed that the feature is an absorption line due to resonant scattering of GRB photons on H-like iron (transition $1s$–$2p$, $E_{\rm rest} = 6.927$ keV). Also, in this case the derived redshift is consistent with that of the host galaxy, and the line width is interpreted as due to the outflow velocity dispersion (up to $0.1c$) of the material, which should have a Fe relative abundance of $\sim$10 with respect to the solar one. In both scenarios, the observed feature points to the presence of an iron-rich environment left by a recent supernova explosion.

GRB 011211 was localized (Gandolfi 2001) with one of the two *BeppoSAX* Wide Field Cameras (WFCs) and promptly followed up with both the *XMM-Newton* satellite and ground-based optical and radio telescopes. In the optical band, a counterpart

[1] Physics Department, University of Ferrara, Via Paradiso 12, 44100 Ferrara, Italy; frontera@fe.infn.it.
[2] Istituto Astrofisica Spaziale e Fisica Cosmica, Sezione di Bologna, CNR, Via Gobetti 101, 40129 Bologna, Italy.
[3] Space Research Organization in the Netherlands, Sorbonnelaan 2, 3584 CA Utrecht, Netherlands.
[4] Institute of Astronomy, University of Cambridge, Madingley Road, Cambridge CB3 0HA, UK.
[5] Department of Astronomy and Astrophysics and Enrico Fermi Institute, University of Chicago, 5640 South Ellis Avenue, Chicago, IL 60637.
[6] Scuola Normale Superiore, Piazza dei Cavalieri 7, I-56100 Pisa, Italy.
[7] Istituto Astrofisica Spaziale e Fisica Cosmica, CNR, Via Fosso del Cavaliere, 00133 Roma, Italy.
[8] Osservatorio Astronomico di Trieste, INAF, Trieste, Italy.

was soon discovered (Grav et al. 2001; Bloom & Berger 2001) and its redshift determined ($z = 2.140 \pm 0.001$; Fruchter et al. 2001; Holland et al. 2002). In the X-ray band, Santos-Lleo et al. (2001) reported the discovery of afterglow emission with *XMM-Newton*, while Reeves et al. (2002, 2003), analyzing the *XMM-Newton* data, reported the evidence of five fading emission lines, which were consistent with blueshifted Kα lines from Mg XI, Si XIV, S XVI, Ar XVIII, and Ca XX outflowing at a velocity of $\sim 0.1c$. However, the significance level of this detection was questioned. Rutledge & Sako (2003), examining the same data analyzed by Reeves et al., found that the claimed lines would not be discovered in a blind search, showing that these features, individually, would be observed in 10% of featureless spectra with the same signal-to-noise ratio.

In the context of a systematic investigation (F. Frontera et al. 2004, in preparation) of the spectral evolution of all GRBs jointly detected with the WFC (Jager et al. 1997) and Gamma-Ray Burst Monitor (GRBM; Frontera et al. 1997; Costa et al. 1998) aboard the *BeppoSAX* satellite, we have analyzed the prompt emission of this burst. Surprisingly, we find marginal evidence of an absorption feature that is visible only during the rise of the event. If true, this is the second case of a transient feature after that observed from GRB 990705. In this paper we report the results of our findings and their possible interpretation.

2. *BeppoSAX* OBSERVATIONS

GRB 011211 was detected with *BeppoSAX* WFC No. 1 and GRBM (Frontera et al. 2002) on 2001 December 11 at 19:09:21 UT. Since a follow-up with *XMM-Newton* was promptly scheduled for this GRB, no observation with the *BeppoSAX* Narrow Field Instruments was performed. The GRB position was determined with an error radius of $2'$ (99% confidence level) and was centered at $\alpha_{2000} = 11^{\rm h}15^{\rm m}16^{\rm s}$ and $\delta_{2000} = -21^\circ 55' 44''$ (Gandolfi 2001).

Data available from the GRBM include two 1 s ratemeters in two energy channels (40–700 keV and >100 keV), 128 s count spectra (40–700 keV, 225 channels), and 40–700 keV counters with very short integration times (from 7.8 ms down to 0.5 ms). The WFC (energy resolution ~20% at 6 keV) were operated in normal mode with 31 channels in 2–28 keV and 0.5 ms time resolution. The burst direction was offset by $9\overset{\circ}{.}1$ with respect to the WFC axis. With this offset, the effective area exposed to the GRB was ~500 cm^2 in the 40–700 keV band and 65 cm^2 in the 2–28 keV energy band. The background in the GRBM energy band was estimated by linear interpolation using the 250 s count rate data before and after the burst. The WFC spectra were extracted through the iterative removal of sources (IROS) procedure[9] (e.g., Jager et al. 1997), which implicitly subtracts the contribution of the background and of other point sources in the field of view.

Among the GRBs simultaneously detected by the *BeppoSAX* WFC and GRBM, GRB 011211 is the longest in both X- (2–28 keV) and gamma-rays (40–700 keV). Figure 1 shows its light curve in these energy bands. In X-rays (Fig. 1, *top panel*) it shows a long rise (~300 s) and a shorter decay (~120 s). Secondary peaks are also visible: three during the GRB rise and one during the burst decay. In gamma-rays (Fig. 1, *bottom panel*), the count statistics do not allow a precise determination of the onset time, which seems to occur later (~100 s) than the onset of the X-ray emission. However, the gamma-ray peak is achieved about 20 s earlier than in X-rays, and the GRB end appears to be simultaneous in X- and gamma-rays. The GRB's entire duration in gamma-rays is ~270 s.

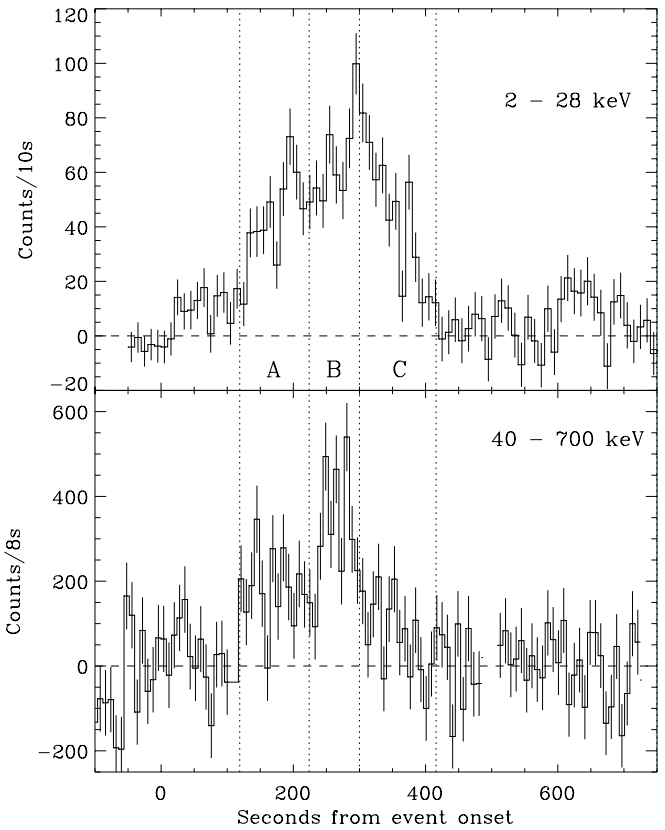

FIG. 1.—Light curve of GRB 011211 in two energy bands, 2–28 keV (WFC) and 40–700 keV (GRBM), after background subtraction. The zero abscissa corresponds to 2001 December 11, 19:04:31 UT. The time slices on which the spectral analysis was performed are indicated by vertical dashed lines.

3. SPECTRAL ANALYSIS AND RESULTS

Following the investigation performed on a sample of *BeppoSAX* GRBs (Frontera et al. 2000), we are performing the systematic analysis of all GRBs detected with the *BeppoSAX* WFC and GRBM in order to study their spectral evolution in the 2–700 keV energy band. Our method is that of subdividing the pulse profile in a certain number of slices of duration in such a way as to derive statistically significant count spectra for each of them. For GRB 011211 we subdivided the light curve into three intervals of 100, 76, and 116 s duration labeled A, B, and C, respectively (see Fig. 1). The derived 2–700 keV count rate spectra are shown in Fig. 2. The surprise was the shape of the spectrum in the time interval A, which showed at a glance, between 6 and 8 keV, a structured depression; this depression was not apparent in the other two spectra, which exhibited the typical shape found in many other GRBs. Subdividing the 100 s interval in two subintervals, the count statistics were very low, but in spite of that, the depression marginally appeared in both spectra. After subdividing the interval B in two subintervals, no trace of the feature was found in either spectra.

The feature in interval A is also evident (see Fig. 3) when we perform the ratio of the GRB count spectra with that of the Crab Nebula, which by chance was observed at an angular offset similar to that of GRB 011211 ($9\overset{\circ}{.}1$). The Crab ratio criterion, commonly used to search for cyclotron resonance features in X-ray pulsars (e.g., Dal Fiume et al. 2000), has the advantage of

[9] WFC software version 105.108.

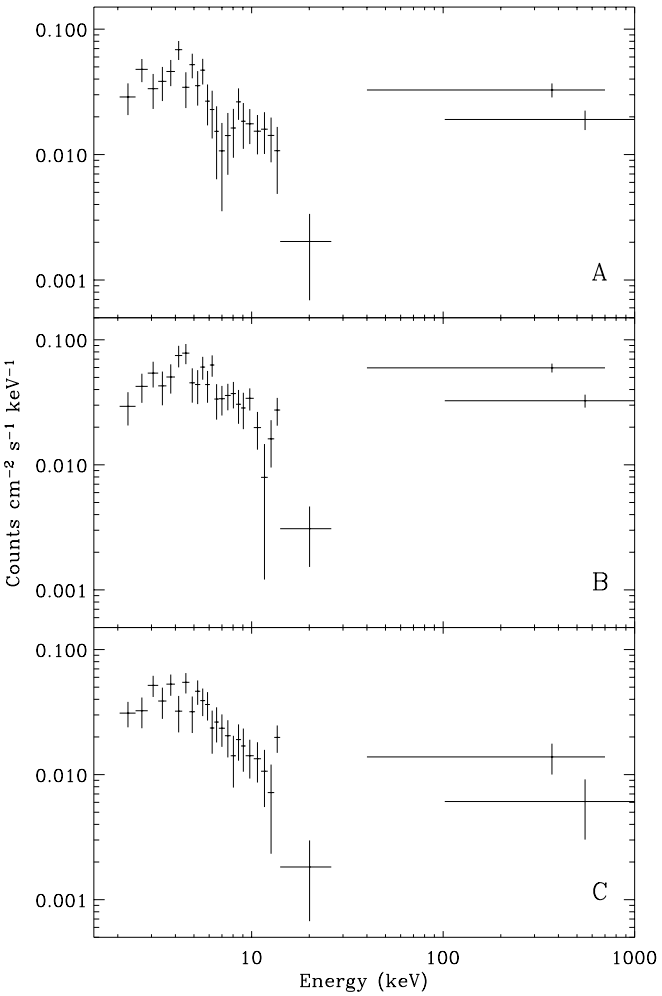

FIG. 2.—Count spectra of the burst in the time intervals A, B, and C.

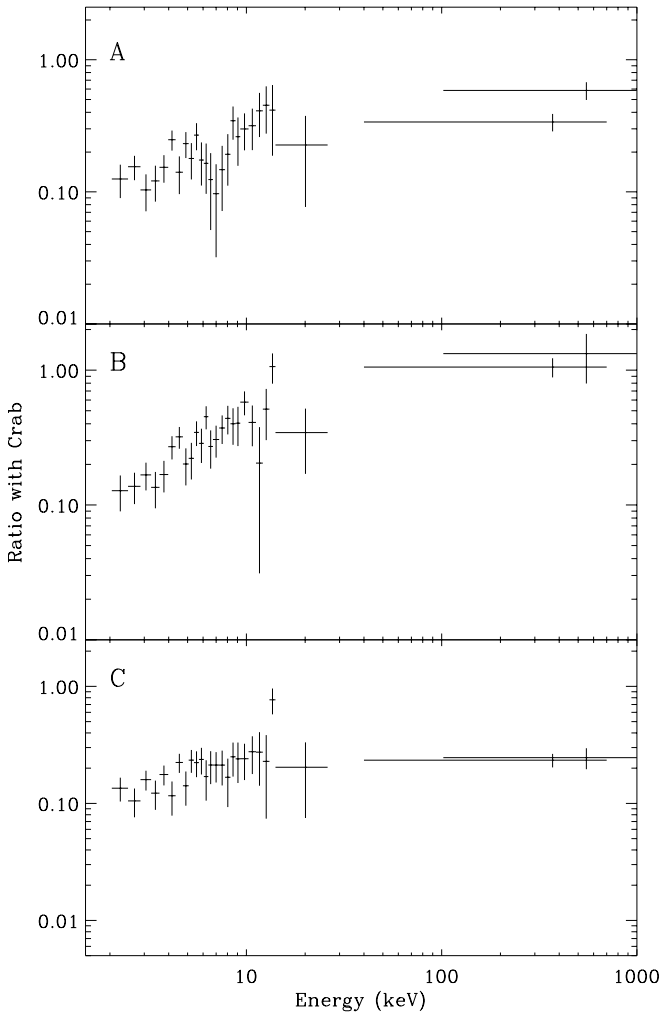

FIG. 3.—Ratio of the WFC spectra in the time intervals A, B, and C to the Crab Nebula spectrum measured by the WFC with the source in the same offset as that of GRB 011211.

being independent of the detector response function adopted and thus minimizing the calibration uncertainties.

We investigated a possible instrumental origin of this depression with negative results. The high voltage, which is monitored every second, does not show any glitch in the interval A. Given the accuracy of the readout (which dominates over statistical noise), this excludes gain changes higher than 0.01%. All the ratemeters show the GRB event, even the ones that measure the illegal events, so there is nothing that can be concluded from them. There are no dips or spikes of any sort, with a typical 3 σ upper limit of 10% per second of measurement (for a count rate of 700 counts s^{-1}). All monitored quantities at the time of the depression do not show anything out of the ordinary. Finally, note that the same procedure was followed to extract both the spectrum A and the spectra B and C, in which the feature is not observed.

As for the other events, the joint WFC and GRBM count rate spectra A, B, and C were analyzed by means of the XSPEC software package (Arnaud 1996). In the fits, allowing the normalization factor of the GRBM data with respect to the WFC data free to vary, we tested various continuum models: power law (PL), broken power law (BKNPL), and smoothly broken power law (or Band law, BL; Band et al. 1993). The PL model provided a good fit only with a GRBM/WFC normalization factor of 0.3, which is unusually low. Indeed, from extended flight calibrations with celestial sources (e.g., the Crab Nebula) and using GRBs observed with both the WFC and GRBM instruments and the *Compton Gamma Ray Observatory* BATSE experiment (e.g., Fishman et al. 1994), this factor was found to range from 0.8 to 1.3. Thus, we excluded the PL model. The BL gave a good fit, but the best-fit parameters derived were not constrained by the data. The best data description and the best parameter constraints were obtained with a BKNPL, with best-fit parameters reported in Table 1. In the fits the GRBM/WFC normalization factor was fixed to 0.8, but we verified that the fit quality and the BKNPL parameter values did not significantly change by using other values of this factor in the 0.8–1.3 range. We also took into account, in the fits, photoelectric absorption of the radiation from the GRB, finding that the equivalent hydrogen column density $N_{\rm H}$ was consistent with zero. Thus, we assumed a Galactic absorption along the GRB direction ($N_{\rm H} = 4.2 \times 10^{20}$ cm^{-2}; Dickey & Lockman 1990).

Even if, for the interval A, the BKNPL model already provides an acceptable fit ($\chi^2/{\rm dof} = 20.4/22$ corresponding to a chance probability of 0.57; see Table 1), the distribution of the residuals from the model (see Fig. 4) still shows evidence of the structured depression. The feature is still apparent in the residuals from the best fits with the other models (PL and BL) and is also evident when only the WFC data are fit with a PL model. The models used are those generally used to describe

TABLE 1

Spectral Parameters of the Best-Fit Models

Parameters	A	B	C
BKNPL			
Γ_1	$1.5^{+0.2}_{-0.7}$	$0.98^{+0.32}_{-0.98}$	$1.50^{+0.21}_{-0.45}$
Γ_2	$1.7^{+0.4}_{-0.2}$	$1.69^{+0.08}_{-0.07}$	$2.26^{+2.21}_{-0.24}$
E_b (keV)	$12.4^{+12.0}_{-8.0}$	$6.9^{+6.1}_{-2.4}$	13^{+49}_{-8}
χ^2/dof	20.4/22	22.1/27	16.4/27
BKNPL Modified by a Negative Gaussian (eq. [1])			
Γ_1	$1.2^{+0.4}_{-0.8}$	$0.95^{+0.35}_{-1.01}$	$1.50^{+0.22}_{-0.47}$
Γ_2	$1.8^{+0.3}_{-0.1}$	$1.69^{+0.08}_{-0.07}$	$2.26^{+2.21}_{-0.24}$
E_b (keV)	$7.4^{+3.5}_{-3.5}$	$6.9^{+6.5}_{-2.7}$	13^{+49}_{-8}
E_L (keV)	$6.9^{+0.6}_{-0.5}$	[6.9]	[6.9]
EW (keV)	$1.2^{+0.5}_{-0.6}$	<0.7 (2σ)	<0.9 (2σ)
χ^2/dof	12.1/20	21.7/26	16.3/26
BKNPL Plus a H-like Fe Resonance Feature			
Γ_1	$1.1^{+0.4}_{-0.8}$	...	...
Γ_2	$1.8^{+0.3}_{-0.1}$	...	...
E_b (keV)	$7.2^{+3.9}_{-3.1}$	...	...
$N_{\rm Fe\ XXVI\ +\ Co\ XXVII}$ ($\rm cm^{-2}$)	$9.4^{+6.9}_{-6.2}\times10^{19}$	...	...
$\beta\gamma$	$1.32^{+0.16}_{-0.16}$	...	...
χ^2/dof	13.1/20	...	...

the prompt continuum emission from GRBs. However, we cannot exclude that a properly tuned two-component continuum model could recover the feature, even if, on the basis of the results obtained thus far in the X-ray band (<10 keV) with *BeppoSAX* and with *HETE-2* (e.g., Barraud et al. 2003), this possibility appears much less probable.

Thus, we decided to evaluate from a statistical point of view the significance of the feature using the residuals from the BKNPL best-fit model. Given that the χ^2-test is a global test, which does not take into account the relative position of the residuals, we performed a null-hypothesis test to check the independence of the residuals around the depression (see Fig. 4). For that we used the run-test (e.g., Bendat & Piersol 1971), a nonparametric test, which is valid independently of the statistics assumed for the data. Taking the residuals to the BKNPL as data points, we investigated the probability that groups of n consecutive data points are mutually independent. Conservatively, the n value was chosen to be the number of energy bins corresponding to 4 times the energy resolution of the instrument in correspondence of the depression region. Thus, we considered values of n ranging from 11 to 14 bins. For a chosen value of n, we scanned the entire count spectrum by moving the first bin of the group. We found that the probability that n consecutive residuals from the BKNPL model are mutually independent ranges from about 0.16 to 0.47 when the energy bins are far from the depression and from 2.7×10^{-3} down to 7.2×10^{-4} (equivalent, in a Gaussian approximation, to 2.8–3.1 σ), depending on n, when the energy bins cover the depression region. The probability values obtained in the depression region for the different values of n are reported in Table 2.

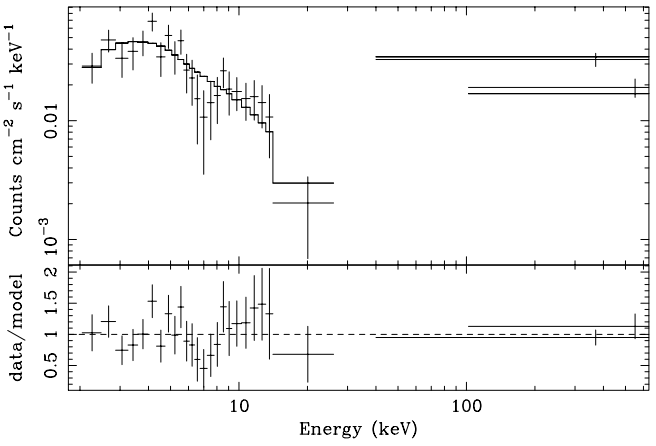

Fig. 4.—*Top*: Count spectrum of GRB 011211 in the time interval A. The steplike curve represents the best fit with a BKNPL. *Bottom*: Distribution of the residuals to the model.

TABLE 2

Probability of Mutually Independent Consecutive Data Points

n	P_r
11	2.1×10^{-3}
12	1.2×10^{-3}
13	7.2×10^{-4}
14	2.7×10^{-3}

Note.—Table lists the probability P_r, obtained with the run-test, that n consecutive data points around the region covered by the depression feature are mutually independent.

Stimulated and encouraged by the run-test results, we replaced the photoelectrically absorbed BKNPL model with the same law modified by a negative narrow Gaussian profile, according to the following equation:

$$N(E) = \begin{cases} A\exp(-\sigma N_{\rm H})E^{-\Gamma_1} \\ \quad\times[1-{\rm EW}G(E;E_l,\sigma_l)] & E\le E_b \\ AE_b^{\Gamma_2-\Gamma_1}E^{-\Gamma_2} \\ \quad\times[1-{\rm EW}G(E;E_l,\sigma_l)] & E\ge E_b, \end{cases} \quad (1)$$

where $\sigma=\sigma(E)$ is the photoelectric cross section of a gas with cosmic abundance (Morrison & McCammon 1983), E_b is the break energy, A is the normalization factor, EW is the equivalent width of the line, and

$$G(E;E_l,\sigma_l) = \frac{1}{\sqrt{2\pi}\sigma_l}\exp\left[\frac{(E-E_l)^2}{2\sigma_l^2}\right] \quad (2)$$

is the assumed Gaussian profile, with centroid energy E_l and standard deviation σ_l. A similar model is, e.g., used to describe cyclotron absorption features from X-ray pulsars (e.g., Soong et al. 1990). The fit results with this new model, instead of the BKNPL, are reported in Table 1. In the fits σ_l is set to 0.1 keV. Leaving it free to vary, the best fit is still obtained for $\sigma_l\approx0.1$ keV with an upper value of 1.2 keV at 90% confidence level. In Figure 5 we show the A spectrum with the best-fit curve and the residuals of the data from the model. As can be seen, the depression has now disappeared ($\chi^2/{\rm dof}=12.1/20$).

Being aware of the warnings given by Protassov et al. (2002) about the use of the F-test for the inclusion of an additional term to a fitting function (Bevington 1969) when this function is an absorption or emission feature, we followed the following

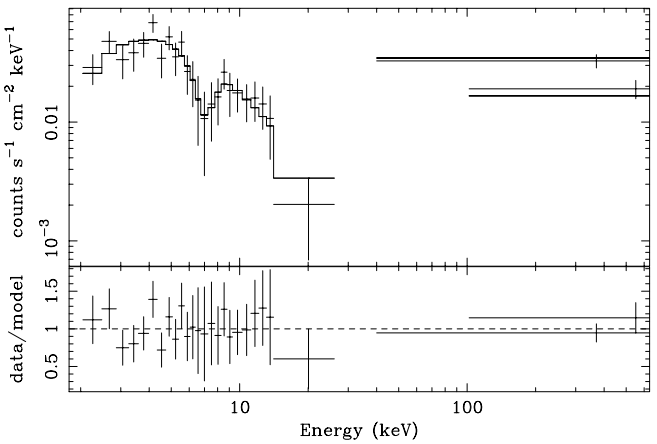

FIG. 5.—*Top*: Photon spectrum of GRB 011211 in the time interval A. The steplike curve represents the best fit with the model given by eq. (1). *Bottom*: Distribution of the residuals to the model.

approach in order to evaluate the probability that the parent fitting function of the spectrum A is actually given by equation (1). Assuming as featureless spectrum the BKNPL model that best fits the WFC plus GRBM data (see Table 1), by means of XSPEC we generated 10,000 WFC fake spectra with the same number of energy bins of the measured A spectrum. These spectra take into account the time duration of the spectrum A, the response function of the instrument, and the Poisson noise associated to the measured spectrum. We fit each of these spectra with a BKNPL model, obtaining a set of 10,000 distributions of residuals from the model assumed. For each of these residual distributions, we performed a blind run-test, determining the spectra that have at least one group of n consecutive residuals from the BKNPL whose probability of being mutually independent is less than the probabilities reported in Table 2. The fraction f_r of the spectra that satisfy this condition are reported in Table 3 for values of n in the range from 11 to 14, as above.

Given that the run-test takes into account the relative position of the residuals but not their amplitude, we also fit these spectra with the equation (1) model, and, mindful of the Protassov et al. (2002) warnings, on these spectra we performed not the F-test for testing the addition of a further component to a fitting function but the one for testing the discrepancy between an assumed fit function and the parent function. This test (see Bevington 1969, p. 195) makes use of the probability distribution of the ratio $F_{12} = \chi^2_{\nu_1}/\chi^2_{\nu_2}$ (or $F_{21} = 1/F_{12}$), where $\chi^2_{\nu_1} = \chi^2/\nu_1$ is obtained from the fit of function 1 (in our case the BKNPL model) to the data, and $\chi^2_{\nu_2} = \chi^2/\nu_2$ is obtained from the fit of function 2 (in our case, eq. [1]).

In the spectral fits with equation (1), the σ_l was again frozen to 0.1 keV, and in order to perform a blind search of a negative Gaussian feature, for each spectrum we performed six fits, each with a different starting value of the feature centroid. In this way we determined the fraction f_t of spectra that satisfy the condition $F_{12} \geq F^m_{12}$, where F^m_{12} is the value measured of F_{12}, derivable from the χ^2 values reported in Table 1. We also checked the condition $F_{21} \leq F^m_{21}$, finding the same result. The values of f_t versus n are reported in Table 3. As can be seen, the fraction of simulated spectra that satisfy both tests ranges from 3×10^{-3} down to 4×10^{-4}. These fractions give our best estimate of the statistical significance of the negative Gaussian feature observed.

TABLE 3

FRACTIONS OF SIMULATED FEATURELESS SPECTRA f_r AND OF TOTAL SPECTRA f_t

n	f_r	f_t
11	0.0262	0.0030
12	0.0103	0.0009
13	0.0044	0.0004
14	0.0244	0.0021

NOTE.—Table lists the fraction of simulated featureless spectra f_r that provide a number of runs with probability $P \leq P_r$ (see Table 2) and the fraction of spectra f_t that satisfy both the above run-test condition and the condition on the F-test (see text).

In the above estimates we did not take into account the number of trials whereby such a feature could be found as a result of a random fluctuation. Thus, assuming that the range of values found for f_t gives the chance probability for a random fluctuation and using the binomial distribution, we evaluated the probability $P(2)$ that, observing n GRBs, two of them (GRB 990705 and GRB 011211) show an absorption feature at their leading edge. To determine n, we selected from the entire sample of GRBs detected with both WFC and GRBM those that show at their leading edge 2–10 keV count spectra with statistical quality at least similar to that of the spectra in the time intervals in which the absorption features are apparent (interval A for GRB 011211, interval B for GRB 990705). We found $n = 18$ and thus $2.4\times10^{-5} \leq P(2) \leq 1.3\times10^{-3}$, depending on the chosen value of the chance probability p, 4×10^{-4} or 3×10^{-3}, respectively. The low values of $P(2)$ gives us an additional confidence that the feature observed is not a random fluctuation, at least on the basis of the GRB sample size obtained with *BeppoSAX*.

Assuming the best-fit centroid energy of the negative Gaussian and $\sigma_l = 0.1$ keV, we also evaluated the 2 σ upper limit to the EW feature in the time intervals B and C. These upper limits and the corresponding χ^2 are also reported in Table 1.

We have also tested a K-edge model (EDGE in XSPEC) in the place of the negative Gaussian. In this case the fit improvement is lower, likely due to the symmetrical shape of the line that does not favor this model.

On the basis of the best-fit results, we have derived the energetics associated with the event. The fluence of the GRB is $S_{2-10} = 1.1\times10^{-6}$ ergs cm^{-2} in the 2–10 keV band, and $S_{40-700} = 5.1\times10^{-6}$ ergs cm^{-2} in the 40–700 keV band, while the total 2–700 keV fluence is $S_{2-700} = 7.5\times10^{-6}$ ergs cm^{-2}. For comparison, in the time interval A (100 s duration), the 2–700 keV fluence is $\sim2.6\times10^{-6}$ ergs cm^{-2}. The peak flux averaged on a 8 s bin is $F^p_{2-10} = 1.56\times10^{-8}$ ergs cm^{-2} s^{-1} in the 2–10 keV band, and $F^p_{40-700} = 5.0\times10^{-8}$ ergs cm^{-2}s^{-1} in the 40–700 keV interval. From the optical redshift, assuming a standard cosmology with $H_0 = 65$ km s^{-1} Mpc^{-1}, $\Omega_\lambda = 0.7$ and $\Omega_m = 0.3$, and isotropic emission, the total fluence corresponds to a released energy of $\sim3.55\times10^{52}$ ergs, with 34% of it released during the first GRB interval. The released energy in the time interval A above 7 keV (feature centroid energy) is 1.2×10^{52} ergs, which corresponds to 98% of the energy released by the burst in this interval.

4. DISCUSSION

There is a long history of X-ray lines from GRBs. In the 1980s, evidence of hard X-ray (>10 keV) absorption features

was reported by Mazets et al. (1981), Hueter (1984), and Murakami et al. (1988). The most significant result was obtained by Murakami et al. (1988) with the Gamma-Ray Burst Detector aboard the *Ginga* satellite, with two transient absorption lines observed during the latest part (5 s duration) of the GRB 880205 leading edge. The line energies were ~19 and ~38 keV, and their chance probability was evaluated to be 6×10^{-5} (Fenimore et al. 1988). Another significant hard X-ray line detection, which was visible, like the previous one, at the leading edge of the burst, was later detected with *Ginga* from GRB 890929 and reported by Yoshida et al. (1991).

All these features at those times had a natural explanation in terms of cyclotron features from Galactic neutron stars (GNS). Once this association with GNS resulted to be untenable owing to the isotropic distribution of GRBs discovered with BATSE, the general belief was that all these features likely were not real. Possible justifications included inaccurate knowledge of the true response functions of the instruments used, partly due to the indetermination of the GRB direction. Another tacit justification was the difficulty of making these lines at cosmological distances. No detection of hard X-ray lines was reported by the BATSE team.

With the advent of the afterglow era, evidence of X-ray lines has been found both in the GRB afterglow and in the prompt emission. Concerning the afterglow, emission lines with energy centroids below 10 keV have been reported from several GRBs (see, e.g., the review by Frontera 2003), most of which point to iron fluorescence or recombination lines from circumburst regions. Concerning the GRB prompt emission, as discussed in § 1, a transient absorption feature was detected during the rise time of GRB 990705 (Amati et al. 2000). In that case, the identification of the absorption feature, either with a K edge of neutral iron (Amati et al. 2000) or with a resonant scattering line of nearly ionized iron (Lazzati et al. 2001), led to a redshift coinciding with the host galaxy redshift independently measured in the optical band (Le Floc'h et al. 2002). This fact strengthened the result.

Now we have the possible evidence of another similar feature from GRB 011211. Also in this case, the feature is visible only during the rise of the primary event. However, in the case of GRB 011211 the interpretation is not so straightforward. First of all, the feature, because of its symmetrical shape, is more consistent with an absorption line than a K edge. In addition, the assumption of a cyclotron resonance feature, which was the assumption for the origin of the *Ginga* lines, appears untenable. If an oriented magnetic field were present in the emitting region, the magnetic field strength can be derived from the condition that the magnetic energy density integrated over the emission region of the prompt emission times a radiative efficiency factor (likely not smaller than ~0.1) is at most equal to the estimated energy released (see § 3). The result is that $B = 10^5 - 10^6$ G. This appears inconsistent with the magnetic field strength ($\sim 10^{12}$ G) obtained assuming that the line is a cyclotron resonance feature ($E_{\rm rest} = 21.7^{+1.9}_{-1.6}$ keV after correcting it for the optically determined redshift). Nor does this large magnetic field seem to be compatible with the value derived from the analysis of the afterglow data (Jakobsson et al. 2003) using the standard homogeneous fireball model (Sari et al. 1998).

The rest-frame energy of the absorption feature is also inconsistent with any plausible resonant scattering line unless we invoke a blueshift of the line. Indeed, the most abundant elements of typical interstellar environments or those typical of a supernova explosion have resonant scattering energies far below the rest-frame energy of the discovered feature (see, e.g., Kato 1976). This implies an absorbing medium with very high outflowing velocities $v_{\rm out}$. A lower limit to this velocity is obtained assuming a resonant scattering of the GRB photons off H-like Ni XXVIII (rest-frame energy of 8.092 keV). To derive the outflow speed, we consider that photons seen in the outflow comoving frame at $\nu = \nu_0$ will be absorbed, where ν_0 is the resonance frequency of the considered line. Therefore, the following condition needs to be satisfied:

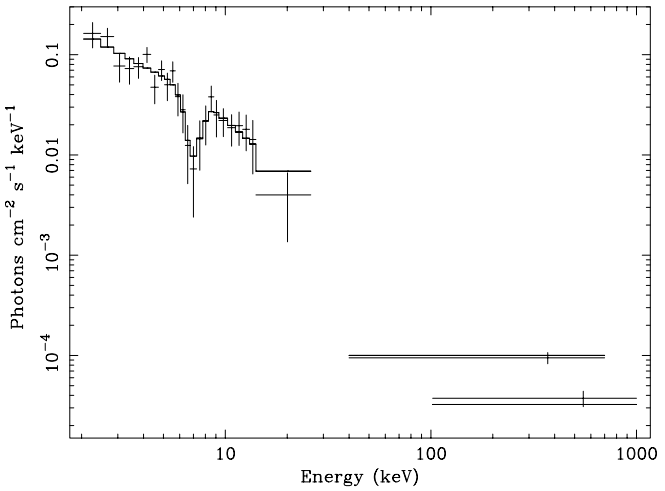

FIG. 6.—*Top*: Photon spectrum of GRB 011211 in the time interval A. The steplike curve represents the best fit with the model used in Lazzati et al. (2001) (see text).

$$(1+z)\delta\nu_{\rm abs} = \nu_0, \tag{3}$$

where $\nu_{\rm abs}$ is the observed absorption frequency and $\delta \equiv [\gamma(1-\beta\cos\theta)]^{-1}$ is the Doppler factor. In our case, since the photon and the fluid direction coincide, we have $\cos\theta = -1$ and the equation can be rewritten, after simple algebra,

$$\frac{1+\beta}{\sqrt{1-\beta^2}} = (1+z)\frac{\nu_{\rm abs}}{\nu_0}, \tag{4}$$

where ν_0 is the rest-frame frequency of the candidate feature. In this case we get $\beta = v_{\rm out}/c = 0.75$ with a corresponding Lorentz factor $\gamma = 1.5$. Note that in this transrelativistic regime neither the $\beta \sim 1$ nor the $\gamma \sim 1$ approximations can be adopted. Equation (4) simplifies, though, to the usual formula $(1+z)\nu_{\rm abs} = 2\gamma\nu_0$ in the ultrarelativistic regime.

Assuming, as proposed by Lazzati et al. (2001) for GRB 990705, that the absorption feature is due to resonant scattering of GRB photons off a mixture of H-like Fe and Co ($E_{\rm rest} =$ 6.927 and 7.518 keV, respectively; oscillator strength of 0.416; Kato 1976), the best fit ($\chi^2/{\rm dof} = 13.1/20$) is obtained assuming a superthermal[10] Gaussian distribution of the product $\beta\gamma$, where γ is the bulk Lorentz factor of the expanding medium, with $\sigma_{\beta\gamma}/(\beta\gamma) = 7.5\%$ and negligible Fe K edge of the absorbing medium. The best-fit parameters of the model (mean value of $\beta\gamma$ and column density of the Fe plus Co absorbing material) are reported in Table 1. From the best-fit value of $\beta\gamma$, we derive, by using equation (4), a value of $\beta = 0.80$ and $\gamma =$ 1.65. The deconvolved spectrum of the interval A with the best-fit model superposed is shown in Figure 6. The low depth

[10] A thermal distribution of outflow velocity would give a resonant feature that is too narrow, since $kT_{\rm Fe} < 10$ keV in order to have a sizable fraction of non–fully ionized iron ions.

of the Fe K edge could be the result of the high ionization level and/or the edge broadening due to Compton scattering (Ross et al. 1999). The disappearance of the feature after $\sim$100 s is likely the result of the inhibition of the electron recombination caused by the increase of the electron temperature as a consequence of inverse Compton heating (Lazzati et al. 2001).

The high outflowing velocity is a problematic issue. The acceleration cannot be due to the interaction with the burst photons themselves, since the feature centroid does not evolve when the interval A is analyzed with higher temporal resolution. A possible explanation is that the absorption feature is due to outflowing material in the line of sight toward the jet cone (see also Königl 2004).

The fit with the physical model allows us to estimate the distance of the absorber and the amount of absorbing material. From equation (12) of Lazzati et al. (2001) we derive

$$R_{\rm abs} \simeq 5 \times 10^{16} \text{ cm}, \quad (5)$$

while the fit yields $N_{\rm Fe+Co} \simeq 10^{20}$ cm^{-2}. Assuming isotropy, the mass of the absorber results in $M_{\rm Fe+Co} = 0.15\ M_{\odot}$, the total mass being $M \sim (60/A_{\rm Fe})\ M_{\odot}$, where $A_{\rm Fe}$ is the iron richness in solar units that is achieved once all the cobalt is decayed into iron. This estimate implies a moderate iron and cobalt enriched material in order to keep the total mass to a reasonable value. Alternatively, one can envisage a clumped material, with a covering factor much lower than unity, with a dense clump lying randomly along the line of sight. In addition, it is possible to derive the total energy involved in the outflow from the best-fit average speed. We obtain $E_{\rm kin} = (\gamma - 1)Mc^2 \sim 5 \times 10^{55}/[A_{\rm Fe}\eta(\Omega/4\pi)]$ ergs, where η is the covering factor of the clumps and Ω is the solid angle within which the material is accelerated to the high speed obtained from the fit. Reasonable values are $A_{\rm Fe} \sim 10$, $\eta \sim 0.1$, and $\Omega/4\pi \sim 0.1$, resulting in a large amount of kinetic energy $E_{\rm kin} \sim 5 \times 10^{52}$ ergs, a value larger than the typical GRB energy of $\sim 10^{51}$ ergs (Bloom et al. 2003).

Given that any absorption feature in the GRB prompt emission, especially during its rise, implies that the absorbing material is external to the fireball, there is only one model among the proposed progenitors that can accommodate this observation. In the supranova scenario (Vietri & Stella 1998) a supernova explodes prior to the GRB, ejecting high-speed material around a newly formed rotating supramassive neutron star. The GRB is produced when the spin of the neutron star is reduced and the compact object collapses to a black hole. In the time span between the supernova and GRB explosions, the spin-down of the neutron star releases $E_{\rm SD} \sim 10^{53}$ ergs, of which a significant fraction could be in the form of a pulsar-type wind. As discussed in Königl & Granot (2002), this energy might be deposited in a pulsar-wind bubble and used to accelerate the supernova shell. They in fact argued that the swept-up remnant is likely to expand anisotropically, with the polar regions of the shell (which can be identified with the gas responsible for the high-energy absorption detected in GRB 011211) attaining speeds $\sim c$.[11] On the other hand, explaining the presence of a large amount of high-velocity absorbing material in the immediate vicinity of the burster is extremely problematic for any model invoking a simultaneous explosion of the burst with the progenitor star (e.g., Woosley 1993), since the stellar wind creates an iron-poor (solar at most), low-density environment at the required distance.

Only more-sensitive X-ray observations than those performed with the *BeppoSAX* WFC can enlarge the GRB sample, improve the statistical quality of the time-resolved spectra, and thus test the results obtained with *BeppoSAX* on the X-ray transient absorption lines. These observations are expected to be only partly covered by the satellite *Swift* (e.g., Krimm 2004), given that these lines are observed only at the leading edge of the bursts, while the *Swift* Burst Alert Telescope has an energy passband from 15 to 150 keV. However, *Swift* can solve the issue of the hard X-ray lines observed with *Ginga*. A sensitive mission that would be able to observe GRBs since their onset and to test the presence of transient X-ray lines with centroid energies below 10 keV could be the proposed Lobster-*ISS* for the *International Space Station*, an all-sky monitor with focusing optics from 0.1 to 3.5 keV (Fraser et al. 2002) paired with a GRB monitor for higher photon energies, from 2 keV to several hundreds of keV (Frontera et al. 2003; Amati et al. 2004).

We wish to thank Nicola Masetti and Eliana Palazzi for useful comments. This research is supported by the Italian Space Agency (ASI) and Ministry of Instruction, University and Research (COFIN funds 2001). *BeppoSAX* was a joint program of ASI and the Netherlands Agency for Aerospace Programs.

[11] In the above picture, the ratio of the distances of the emission and absorption regions of the remnant, $R_{\rm em}/R_{\rm abs}$, would be approximately equal to the ratio of their respective expansion speeds ($\sim 0.1/0.8$ in this case). Using eq. (3), this yields $R_{\rm em} \sim 6 \times 10^{15}$ cm.

REFERENCES

Amati, L., et al. 2000, Science, 290, 953
———. 2004, paper presented at the 35th COSPAR Symposium
Arnaud, K. A. 1996, in ASP Conf. Ser. 101, Astronomical Data Analysis Software and Systems V, ed. G. H. Jacoby & J. Barnes (San Francisco: ASP), 17
Band, D., et al. 1993, ApJ, 413, 281
Barraud, C., et al. 2003, A&A, 400, 1021
Bendat, J. S., & Piersol, A. G. 1971, Random Data: Analysis and Measurement Procedures (New York: Wiley)
Bevington, P. R. 1969, Data Reduction and Error Analysis for the Physical Sciences (New York: McGraw-Hill)
Bloom, J. S., & Berger, E. 2001, GCN Circ. 1193, http://gcn.gsfc.nasa.gov/gcn3/1193.gcn3
Bloom, J. S., Frail, D. A., & Kulkarni, S. R. 2003, ApJ, 594, 674
Böttcher, M. 2000, ApJ, 539, 102
Böttcher, M., Dermer, D. D., Crider, W., & Liang, E. P. 1999, A&A, 343, 111
Costa, E., et al. 1998, Adv. Space Res., 22, 1129
Dal Fiume, D., et al. 2000, Adv. Space Res., 25, 399
Dickey, J. M., & Lockman, F. J. 1990, ARA&A, 28, 215
Fenimore, E. E., et al. 1988, ApJ, 335, L71
Fishman G. J., et al. 1994, ApJS, 92, 229
Frail, D., et al. 2001, ApJ, 562, L55
Fraser, G., et al. 2002, Proc. SPIE, 4497, 115
Frontera, F. 2003, in Supernovae and Gamma Ray Bursters, ed. K. W. Weiler (New York: Springer), 317
Frontera, F., et al. 1997, A&AS, 122, 357
———. 2000, ApJS, 127, 59
———. 2002, GCN Circ. 1215, http://gcn.gsfc.nasa.gov/gcn3/1215.gcn3
———. 2003, talk presented at the Third National Conference on Astrophysics of Compact Objects
Fruchter, A., Vreeswijk, P., Rhoads, J., & Burud, I. 2001, GCN Circ. 1200, http://gcn.gsfc.nasa.gov/gcn3/1200.gcn3
Gandolfi, G. 2001, GCN Circ. 1189, http://gcn.gsfc.nasa.gov/gcn3/1189.gcn3
Grav, T., et al. 2001, GCN Circ. 1191, http://gcn.gsfc.nasa.gov/gcn3/1191.gcn3
Hjorth, J., et al. 2003, Nature, 423, 847

Holland, S. T., et al. 2002, AJ, 124, 639
Hueter, G. J. 1984, in High Energy Transients in Astrophysics, ed. S. Woosley (New York: AIP), 373
Jager, R., et al. 1997, A&AS, 125, 557
Jakobsson, P., et al. 2003, A&A, 408, 941
Kato, T. 1976, ApJS, 30, 397
Königl, A. 2004, in ASP Conf. Proc. 312, Third Rome Workshop on Gamma-Ray Bursts in the Afterglow Era, ed. M. Feroci, F. Frontera, N. Masetti, & L. Piro (San Francisco: ASP), 333
Königl, A., & Granot, J. 2002, ApJ, 574, 134
Krimm, H. A. 2004, NewA Rev., 48, 551
Lazzati, D., Campana, S., & Ghisellini, G. 1999, MNRAS, 304, L31
Lazzati, D., & Perna, R. 2002, MNRAS, 330, 383
Lazzati, D., et al. 2001, ApJ, 556, 471
Le Floc'h, E., et al. 2002, ApJ, 581, L81
Mazets, E. P., et al. 1981, Nature, 290, 378
Morrison, R., & McCammon, D. 1983, ApJ, 270, 119
Murakami, T., et al. 1988, Nature, 335, 234
Paczynski, B. 1998, ApJ, 494, L45
Perna, R., & Loeb, A. 1998, ApJ, 501, 467
Protassov, R., et al. 2002, ApJ, 571, 545
Reeves, J. N., et al. 2002, Nature, 416, 512
———. 2003, A&A, 403, 463
Ross, R. R., Fabian, A. C., & Young, A. J. 1999, MNRAS, 306, 461
Rutledge, R. E., & Sako, M. 2003, MNRAS, 339, 600
Santos-Lleo, M., Loiseau, N., Rodriguez, P., Altieri, B., & Schartel, N. 2001, GCN Circ. 1192, http://gcn.gsfc.nasa.gov/gcn3/1192.gcn3
Sari, R., Priran, T., & Narayan, R. 1998, ApJ, 497, L17
Soong, Y., et al. 1990, ApJ, 348, 641
Stanek, K. Z., et al. 2003, ApJ, 591, L17
Vietri, M., & Stella, L. 1998, ApJ, 507, L45
Wang, L., et al. 2003, ApJ, 592, 457
Weth, C., Meszaros, P., Kallman, T., & Rees, M. 2000, ApJ, 534, 581
Woosley, S. 1993, ApJ, 405, 273
Yoshida, A., et al. 1991, PASJ, 43, L69